QUANTUM SIMULATION

Spin- and density-resolved microscopy of antiferromagnetic correlations in Fermi-Hubbard chains

Martin Boll,[1]* Timon A. Hilker,[1]* Guillaume Salomon,[1]* Ahmed Omran,[1] Jacopo Nespolo,[2] Lode Pollet,[2] Immanuel Bloch,[1,2] Christian Gross[1]†

The repulsive Hubbard Hamiltonian is one of the foundational models describing strongly correlated electrons and is believed to capture essential aspects of high-temperature superconductivity. Ultracold fermions in optical lattices allow for the simulation of the Hubbard Hamiltonian with control over kinetic energy, interactions, and doping. A great challenge is to reach the required low entropy and to observe antiferromagnetic spin correlations beyond nearest neighbors, for which quantum gas microscopes are ideal. Here, we report on the direct, single-site resolved detection of antiferromagnetic correlations extending up to three sites in spin-1/2 Hubbard chains, which requires entropies per particle well below $s^* = \ln(2)$. The simultaneous detection of spin and density opens the route toward the study of the interplay between magnetic ordering and doping in various dimensions.

The Fermi-Hubbard model, which describes interacting fermions on a lattice, supports a rich phase diagram at low temperatures. Despite the conceptual simplicity of the Hubbard model, parts of its phase diagram, especially away from half-filling, and its connection to high-temperature superconductivity are still under debate (*1*). Controlled experiments with ultracold fermions in optical lattices might provide new insight (*2*). For one particle per lattice site, the so-called half-filling regime of a balanced two-component fermion mixture, and repulsive interactions, the Hubbard model features a crossover from a metallic to a Mott insulating state when the temperature is lowered. For even lower temperatures, antiferromagnetic correlations are expected to develop in the Mott insulating phase owing to the superexchange mechanism (*2*–*5*). The paramagnetic Mott insulating state has been observed in seminal ultracold atom experiments involving trap-averaged quantities and, recently, at the single-atom level (*6*–*12*). Detailed experimental studies of the thermodynamics of the Hubbard model also revealed its equation of state in the density sector down to temperatures at which short-range spin-ordering might occur (*13*, *14*). Unfortunately, the experimental preparation of low-entropy lattice fermions has proven to be extremely challenging, making the observation of longer ranged antiferromagnetism difficult. Important progress in revealing magnetic ordering in the Hubbard model has been reported with the observation of nearest-neighbor correlations via singlet-triplet spin oscillations (*15*–*17*) and short-range correlations deduced from optical Bragg spectroscopy (*18*). However, the detection of the onset of magnetic order is complicated by the inhomogeneity of the trapped samples, in which different phases coexist. Microscopic control or detection helps to overcome this limitation, and the analog of antiferromagnetic correlations has been measured in small systems of up to three fermions (*19*). Recently, local non–spin-resolved detection of ultracold fermions in single-lattice sites has been demonstrated (*20*–*23*), and the nonuniform entropy distribution in band and Mott insulating states has been observed in the density sector (*11*, *12*, *24*).

Here, we report on a site- and spin-resolved study of antiferromagnetic correlations extending over up to three sites in one-dimensional (1D) spin-1/2 Hubbard chains realized with ultracold lithium-6 in an optical superlattice. Using our spin and onsite atom number–sensitive quantum gas microscope, we directly measured spin correlations together with density fluctuations in the system.

The fermionic atoms in each of the 1D lattice tubes are well described by the single-band Hubbard Hamiltonian

$$\hat{H} = -t\sum_{i,\sigma}(\hat{c}^{\dagger}_{i,\sigma}\hat{c}_{i+1,\sigma} + \text{h.c.}) + U\sum_{i}\hat{n}_{i,\uparrow}\hat{n}_{i,\downarrow} + \sum_{i,\sigma}\varepsilon_i\hat{n}_{i,\sigma} \quad (1)$$

Here, the fermion creation operator is denoted by $\hat{c}^{\dagger}_{i,\sigma}$ and the annihilation operator is denoted by $\hat{c}_{i,\sigma}$ at site i for each of the two spin states $\sigma = \uparrow,\downarrow$. The operator $\hat{n}_{i,\sigma} = \hat{c}^{\dagger}_{i,\sigma}\hat{c}_{i,\sigma}$ counts the number of atoms with spin σ on the respective site. Three competing energy scales govern the physics of this system: intersite nearest-neighbor hopping with strength t, onsite interactions of strength U, and local trap-induced energy offsets ε_i. Here, t is controlled via the lattice depth, whereas U can be tuned independently in the experiment by using the broad Feshbach resonance of lithium-6 between the lowest hyperfine states $|\downarrow\rangle = |F = 1/2, m_F = -1/2\rangle$ and $|\uparrow\rangle = |1/2, 1/2\rangle$ (*25*), where F and m_F define the hyperfine state of the atoms. In the experiments reported here, we exclusively worked with repulsive interactions $U > 0$, for which the Hubbard model supports finite-range antiferromagnetism with correlations suddenly appearing at distances beyond nearest neighbors for entropies per particle below the "critical" value of $s^* = S/Nk_B = \ln(2)$ (*26*–*28*), where S is the entropy, N is the atom number, and k_B is the Boltzmann constant. True long-range order is absent in the 1D Hubbard model even at zero temperature (*4*, *29*), and the algebraic decay of the correlations is strong even on a distance of a few sites (*27*, *28*). In the limit of very strong repulsive interactions and half-filling, the emerging spin order is intuitively understood from the mapping of the Hubbard model to a Heisenberg antiferromagnet with superexchange coupling $J = 4t^2/U$ (*3*). For weaker interactions, particle-hole fluctuations become important, and the ground state is characterized by a spin density wave. In one dimension, the model is Bethe ansatz integrable (*4*, *29*), and precise predictions for the finite entropy spin correlations and density fluctuations have been reported in the parameter regime relevant to cold-atom experiments (*27*, *28*).

The experiments started with the preparation of a low-temperature balanced spin mixture of the $|\uparrow\rangle$ and $|\downarrow\rangle$ states in a single 2D lattice plane (*24*). The final temperature and atom number was controlled by magnetic field–driven spill-out evaporation at repulsive interactions (*30*). We set the final interaction strength using a homogeneous magnetic offset field in order to control the scattering length in the vicinity of the Feshbach resonance centered at 832 G (*25*). Afterward, we ramped up the large spacing component (site separation $a_{sl} = 2.3$ μm) of a superlattice (*31*, *32*) in the y direction to prepare independent 1D tubes. Next, we slowly turned on a lattice with spacing $a_l = 1.15$ μm along the tubes in the x direction using a 100-ms linear ramp to 11 E_R, where $E_R = \hbar^2/8ma_l^2$ denotes the recoil energy of the lattice for atoms of mass m and $\hbar$ is Planck's constant. The hopping strength is $t = \hbar \times 125(9)$ Hz at this final lattice depth. The lattice filling was controlled by varying the evaporation parameters. To simultaneously detect the spin and density degrees of freedom of the 1D Hubbard chains locally, we froze the dynamics by rapidly increasing the lattice depth along the tubes to 42 E_R within 1 ms, followed by a turn-off of the magnetic offset field in 20 ms. We obtained spin resolution using the superlattice potential and a magnetic field gradient in the y direction in a Stern-Gerlach–like setting. The magnetic field gradient shifted the potential minima experienced by the two spin states of opposite magnetic moment, and the subsequent adiabatic ramp-up of the short scale component of the y superlattice with well separation a_l caused a separation of the spins into the two different sites of the local double well (Fig. 1A). Applying this technique to a spin-polarized gas,

[1]Max-Planck-Institut für Quantenoptik, 85748 Garching, Germany. [2]Fakultät für Physik, Ludwig-Maximilians-Universität, 80799 München, Germany.
*These authors contributed equally to this work. †Corresponding author. Email: christian.gross@mpq.mpg.de

we inferred a splitting fidelity of 98% limited by superlattice phase fluctuations of 25 mrad (*30*). Last, we ramped up a 3D pinning lattice for detection and reconstructed the lattice site occupations from fluorescence images (Fig. 1, B and C) after deconvolution with the measured point-spread-function (*24*, *30*). The above detection procedure enables us to detect the position of all spins, doublons, and holes in the system with single-lattice-site resolution, obtaining complete information about the system in Fock space.

First, we analyzed the spin correlations $C(d) = 4(\langle \hat{S}_i^z \hat{S}_{i+d}^z \rangle - \langle \hat{S}_i^z \rangle \langle \hat{S}_{i+d}^z \rangle)$ between the spin operators $\hat{S}_i^z = \frac{\hat{n}_{i,\uparrow} - \hat{n}_{i,\downarrow}}{2}$ versus distance d. To this end, we fixed the s wave scattering length to $671(10)a_B$, where a_B is the Bohr radius, corresponding to $U/t = 12.6$ and took a high statistics data set of 1200 individual pictures. We focused on the central region of the inhomogeneous sample, defining two spatial regions of interest for the analysis. The first one, referred to as the loose filter, involves all sites with an average density $\hat{n}_i = \hat{n}_{i,\uparrow} + \hat{n}_{i,\downarrow}$ in the range $\hat{n}_i = 1 \pm 0.3$. Here, we benefit from higher statistics, but there is a considerable effect of lower-density regions in the data. The second, so-called tight filter selects one specific tube and takes into account only sites closer to unity density with $\hat{n}_i = 1 \pm 0.1$ (*30*). The strong nearest-neighbor correlations of $C(1) = -0.220(5)$ and $C(1) = -0.34(9)$ observed for the loose and tight filtering correspond to 37 and 58%, respectively, of the expected zero-temperature signal in the Heisenberg limit (Fig. 2) (*27*, *28*). These data are based on the average over all measurements taken for $U/t > 8$ (Fig. 3). We observed significant correlations over a distance of up to three sites of the staggered correlator $C_s(d) = (-1)^d C(d)$. A comparison between the experimentally measured correlator $C(d)$ and finite-temperature quantum Monte Carlo (QMC) calculations for homogeneous Hubbard chains at half-filling allows the determination of the entropy and temperature of the lattice gas (*30*). We inferred an effective local entropy per particle of $s = 0.61(1)$ in the loosely filtered case, reducing to $s = 0.51(5)$ for the tight filter, both significantly below $s^* = \ln(2) \approx 0.69$. In a uniform system at half-filling, this lowest entropy corresponds to a temperature of $k_B T/t = 0.22(4)$ at $U/t = 12.6$ (*30*).

In order to explore the properties of the Hubbard chains at different interaction strengths U/t, we measured spin correlations and particle-hole fluctuations for varying onsite interactions U, while keeping the lattice ramp and final lattice depth constant at 11 E_R (Fig. 3). We compared the measurements to QMC results for a homogeneous system at half-filling for different temperatures and entropies. The dependence of the correlations on the interactions is rather different when comparing isothermal and isentropic state preparation. In the former case, a maximum of the correlations is expected at intermediate interactions U/t, where part of the entropy is carried by density modes (*33*), whereas at large interactions, the correlations decrease owing to the smaller energy scale of spin excitations given by the superexchange coupling J. In the isentropic case of constant entropy, spin correlations saturate toward strong interactions, where the energetic gap between spin and density modes is large. At intermediate interaction strengths, the correlation behavior depends on the entropy, and a weakly pronounced maximum exists for intermediate entropies around $s^* = \ln(2)$ (Fig. 3A), whereas below $s = 0.6$, a monotone increase of the correlations with interaction strength is expected. Experimentally, we observed a saturation behavior of the spin correlations for $U/t > 8$. The inferred temperature dropped from $k_B T = 0.6t$ to $0.3t$ while increasing U/t from 8 to 16, as expected for adiabatic cooling. At intermediate interactions, $U/t \approx 5$, we observed reduced spin

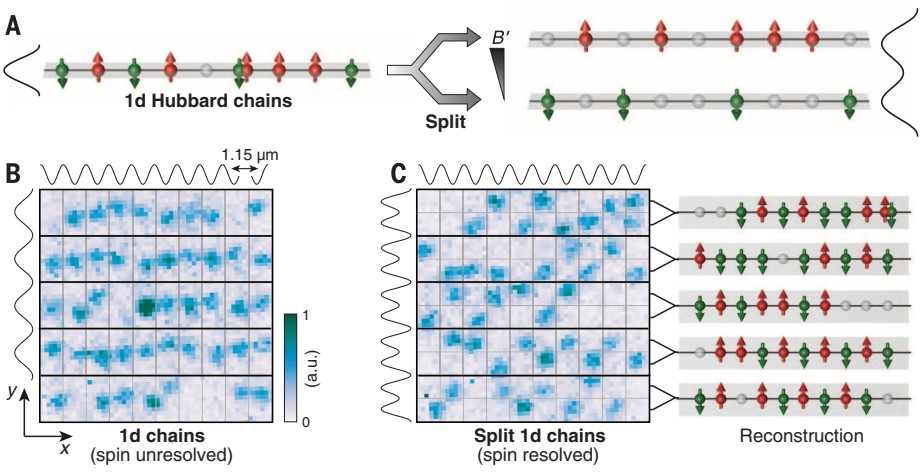

Fig. 1. Schematic of the spin- and density-resolved detection. (**A**) Schematic of the spin-resolved imaging. Each site of the Hubbard chain was split spin-dependently into a local double-well potential by applying a magnetic field gradient B'. This allows for the simultaneous detection of up spins ($|\uparrow\rangle$, red), down spins ($|\downarrow\rangle$, green), doublons (up and down spins overlapping), and holes (gray spheres) and thus for a full characterization of the Hubbard chains. (**B**) Typical fluorescence image of atoms in five mutually independent 1D tubes imaged before splitting. The lattice potentials are indicated by the black lines next to the images, with a spacing along the tubes oriented in the x direction of 1.15 μm and a transverse intertube separation of 2.3 μm. The increasing fluorescence level is shown by darker colors in relative units (color bar). The imaging slightly displaces the atoms from their original positions and also allows for the detection of doubly occupied sites (saturated signal in the center) (*24*). (**C**) Typical image with spin-resolved detection. A superlattice in the y direction (indicated on the left of the image) was used to split each chain in a spin-dependent manner. The $|\downarrow\rangle$ spins were pulled down, whereas the $|\uparrow\rangle$ spins were pulled upward. (Right) Illustration of the reconstructed Hubbard chains.

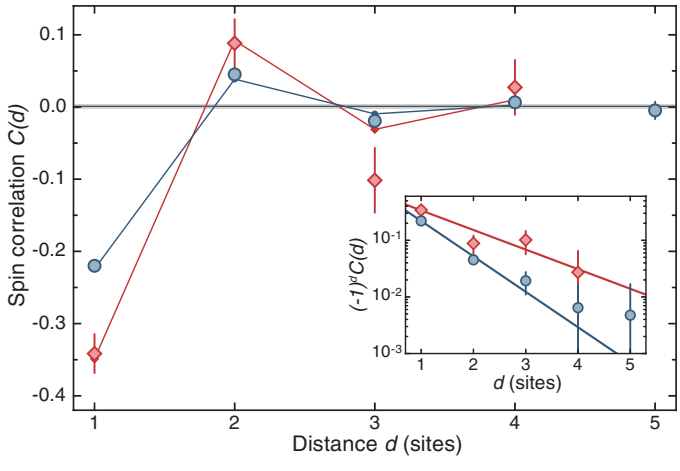

Fig. 2. Antiferromagnetic spin correlations versus distance. Measured spin correlations at $U/t = 12.6$ for the loosely (blue circles) and more tightly filtered data (red diamonds). The staggered behavior directly visualizes the antiferromagnetic nature of the correlations $C(d)$. Correlations up to three sites are statistically significant. The transverse correlations (gray line) vanish within their 1 SEM uncertainty (light gray shading). The red and blue lines connecting filled symbols are QMC results for a homogeneous system at half-filling corresponding to entropies per particle of $s = 0.51(5)$ and $s = 0.61(1)$, respectively. (Inset) Decay of the staggered spin correlator $C_s(d) = (-1)^d C(d)$ in a logarithmic plot together with an exponential fit $C_s(d) \propto \exp(-d/\xi)$, revealing decay lengths of $\xi = 0.69(6)$ sites and $\xi = 1.3(4)$ sites for the two data sets. For low entropies, an exponential decay is expected to be strictly valid only at large distances. However, within the statistical uncertainty of the experimental data, the fit captures the observed behavior. All error bars represent 1 SEM.

correlations compared with the isentropic prediction at half-filling. We attribute this to a changing entropy distribution in the trap (*8*, *30*) and a measured weak increase of the mean density in the analyzed region by 5%. In the regime of saturated spin correlations, the doublon and hole fractions reached their lowest value of P_d = 5% and P_h = 12%, respectively. The higher hole fraction is mainly caused by the loose filtering, which results in an effective hole doping in the analyzed region of the system; this doping is lower (P_d = 3%, P_h = 7%) for the tightly filtered data.

More insight into the behavior of the spin correlations can be obtained by making use of the full microscopic characterization of the system. To study the antiferromagnetic spin correlations away from half-filling, we show the nearest neighbor correlator $C(1)$ per pair of sites versus their mean density in Fig. 4. These data combine different data sets taken at U/t = 10.3 and also contain measurements at different temperatures, obtained by holding the cloud for up to 2.5 s in the 2D plane. We observed a clear dependence of the spin correlator on the local density, with strongest correlations close to $\langle \hat{n} \rangle = 1$. Away from half-filling, both to higher and lower densities, a strong decrease of the correlations is observed, reflecting that doping reduces spin order (*2*). Generally, the data scatter is much higher than expected just by statistics—that is, at a given density we observe events with a range of significantly different nearest-neighbor spin correlations. This reflects the distribution of entropy within each cloud, as well as between the measurement settings. To further analyze the data, we selected a density interval $\langle \hat{n}_i \rangle = 1 \pm 0.1$ and calculated the normalized variance of the density $\mathrm{Var}(\hat{n})/\langle \hat{n} \rangle$ for all pairs of sites in this window. These fluctuations reflect the entropy in the density sector, whereas the nearest-neighbor spin correlations are a measure of the spin entropy. We show their mutual dependence in the inset of Fig. 4, identifying two distinct regimes of total entropy. In the regime below $s^* = \ln(2)[C(1) \lesssim -0.15]$, the density fluctuations depend only weakly on the total entropy (*27*, *28*), which in turn is stored in the spin fluctuations. Only when these are saturated at s^* do the density fluctuations grow, visible in their steep rise when the spin correlations are just below zero. The freezing of density fluctuations renders them useless as a thermometer in the low-entropy regime, whereas the highly temperature-sensitive (and entropy-sensitive) spin correlations are ideal for this purpose down to T = 0 (*27*).

Such a "spin thermometer" (*30*, *34*) is a crucial step toward optimized cooling (*35*, *36*) to lower entropies required to study, for example, d wave superfluidity away from half-filling (*37*). The demonstrated measurement of all relevant degrees of freedom gives access to spin-density correlators, which are essential to reveal the interplay of magnetism and doping. Furthermore, the combination of superlattices and local detection will allow for the search of an adiabatic path between low-entropy valence bond solids (*15*) or plaquette-resonating valence bond states (*38*, *39*) and the Heisenberg antiferromagnet (*40*),

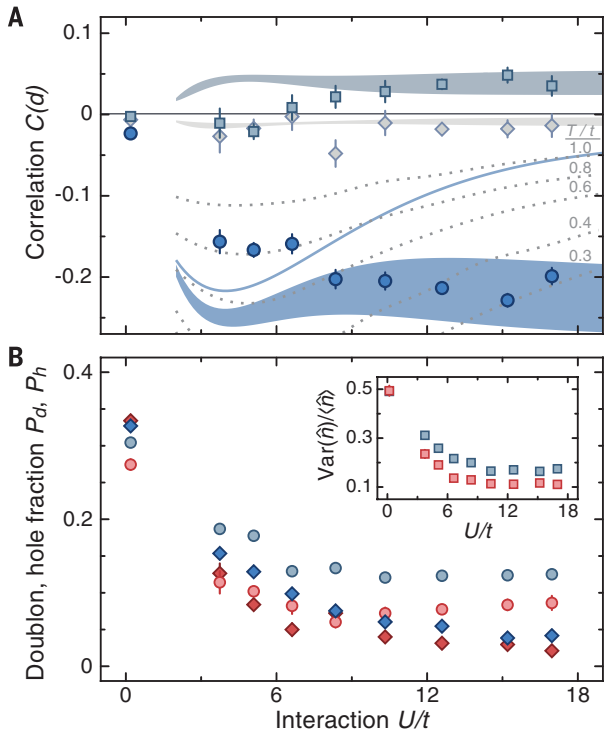

Fig. 3. Spin and density degrees of freedom at different interaction strengths. (**A**) Spin correlations $C(d)$ for distances d = 1 (dark blue), 2 (light blue), and 3 (gray) versus interaction strength U/t. Starting close to zero at vanishing interactions, finite range spin correlations develop and saturate for interaction strengths $U/t > 8$. The shaded areas indicate the QMC predictions in a homogeneous system at half-filling for an entropy per particle between s = 0.60 (lower bound) and 0.65 (upper bound); the solid line is the prediction for $C(1)$ at $s^* = \ln(2)$. Dotted lines are isothermals for $C(1)$ at the indicated temperatures. For large U/t, we observed adiabatic cooling, whereas both temperature and entropy decrease in the analyzed spatial region at intermediate U/t. The transverse nearest-neighbor correlations (dark gray line close to zero) is consistently above the d = 3 spin correlator, which supports its statistical significance. Because of limited statistics, only loosely filtered data is shown. (**B**) Evolution of the density degree of freedom. Shown is the evolution of the fraction of holes (circles) and doublons (diamonds) with interaction strength U/t. The hole (P_h) and doublon (P_d) fractions decrease for stronger interactions and then saturate. Data are shown for the loose (blue) and tight (red) filter cases. (Inset) Evolution of the normalized onsite atom number variance $\mathrm{Var}(\hat{n})/\langle \hat{n} \rangle$ The density fluctuations are suppressed already at vanishing interactions owing to effects of Pauli blocking in the metal. This suppression becomes stronger for increasing interactions until the fluctuations saturate. All error bars represent 1 SEM, and the apparent fluctuation of the data are due to day-to-day systematics.

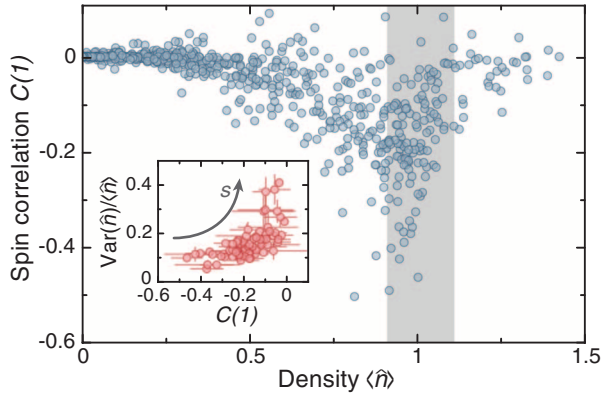

Fig. 4. Interplay of density and spin fluctuations. We show the nearest-neighbor spin correlations $C(1)$ for different densities corresponding to different positions in the trap. The data combine several measurements at an interaction strength of U/t = 10.3, also including higher-temperature data. Every data point corresponds to two neighboring sites, where between 30 and 2000 samples contribute. The strength of spin correlations $C(1)$ peaks just below densities of one is consistent with the half-filling regime taking the detection efficiency of ~95% into account. (Inset) The normalized density fluctuations $\mathrm{Var}(\hat{n})/\langle \hat{n} \rangle$ versus $C(1)$ for a density interval $\langle \hat{n}_i \rangle = 1 \pm 0.1$ as indicated by the gray area in the main plot. Density fluctuations rise steeply for low values of the spin correlator, signaling the saturation of the entropy in the spin sector. This characteristic dependence identifies the strong vertical scatter of the data in the main figure mainly as a result of different local entropies s as indicated by the arrow. For clarity of the presentation, we omit the error bars in the main figure. They are of the same size as the ones in the inset and correspond to 1 SEM.

also in two dimensions. Realization of the paradigmatic quantum phase transition from such an artificial valence bond solid to a Heisenberg antiferromagnet (*41*) therefore seems within reach of present experiments.

Recently, we became aware of similar experimental results in two dimensions (*42*, *43*).

REFERENCES AND NOTES

1. P. W. Anderson, *Science* **235**, 1196–1198 (1987).
2. K. L. Hur, T. M. Rice, *Ann. Phys.* **324**, 1452–1515 (2009).
3. A. Auerbach, *Interacting Electrons and Quantum Magnetism* (Springer Science & Business Media, 1994).
4. T. Giamarchi, *Quantum Physics in One Dimension* (Clarendon, 2004).
5. T. Esslinger, *Ann. Rev. Condens. Matter Phys.* **1**, 129–152 (2010).
6. R. Jördens, N. Strohmaier, K. Günter, H. Moritz, T. Esslinger, *Nature* **455**, 204–207 (2008).
7. U. Schneider *et al.*, *Science* **322**, 1520–1525 (2008).
8. R. Jördens *et al.*, *Phys. Rev. Lett.* **104**, 180401 (2010).
9. S. Taie, R. Yamazaki, S. Sugawa, Y. Takahashi, *Nat. Phys.* **8**, 825–830 (2012).
10. P. M. Duarte *et al.*, *Phys. Rev. Lett.* **114**, 070403 (2015).
11. D. Greif *et al.*, *Science* **351**, 953–957 (2016).
12. L. W. Cheuk *et al.*, *Phys. Rev. Lett.* **116**, 235301 (2016).
13. C. Hofrichter *et al.*, *Phys. Rev. X* **6**, 021030 (2016).
14. E. Cocchi *et al.*, *Phys. Rev. Lett.* **116**, 175301 (2016).
15. S. Trotzky, Y.-A. Chen, U. Schnorrberger, P. Cheinet, I. Bloch, *Phys. Rev. Lett.* **105**, 265303 (2010).
16. D. Greif, T. Uehlinger, G. Jotzu, L. Tarruell, T. Esslinger, *Science* **340**, 1307–1310 (2013).
17. D. Greif, G. Jotzu, M. Messer, R. Desbuquois, T. Esslinger, *Phys. Rev. Lett.* **115**, 260401 (2015).
18. R. A. Hart *et al.*, *Nature* **519**, 211–214 (2015).
19. S. Murmann *et al.*, *Phys. Rev. Lett.* **115**, 215301 (2015).
20. L. W. Cheuk *et al.*, *Phys. Rev. Lett.* **114**, 193001 (2015).
21. M. F. Parsons *et al.*, *Phys. Rev. Lett.* **114**, 213002 (2015).
22. E. Haller *et al.*, *Nat. Phys.* **11**, 738–742 (2015).
23. G. J. A. Edge *et al.*, *Phys. Rev. A* **92**, 063406 (2015).
24. A. Omran *et al.*, *Phys. Rev. Lett.* **115**, 263001 (2015).
25. G. Zürn *et al.*, *Phys. Rev. Lett.* **110**, 135301 (2013).
26. J. Sirker, A. Klümper, *Phys. Rev. B* **66**, 245102 (2002).
27. E. V. Gorelik *et al.*, *Phys. Rev. A* **85**, 061602 (2012).
28. B. Sciolla *et al.*, *Phys. Rev. A* **88**, 063629 (2013).
29. F. H. L. Essler, H. Frahm, F. Göhmann, A. Klümper, V. E. Korepin, *The One-Dimensional Hubbard Model* (Cambridge Univ. Press, 2005).
30. Supplementary text is available as supplementary materials on *Science* Online.
31. J. Sebby-Strabley, M. Anderlini, P. Jessen, J. Porto, *Phys. Rev. A* **73**, 033605 (2006).
32. S. Fölling *et al.*, *Nature* **448**, 1029–1032 (2007).
33. F. Werner, O. Parcollet, A. Georges, S. R. Hassan, *Phys. Rev. Lett.* **95**, 056401 (2005).
34. R. Olf, F. Fang, G. E. Marti, A. MacRae, D. M. Stamper-Kurn, *Nat. Phys.* **11**, 720–723 (2015).
35. J.-S. Bernier *et al.*, *Phys. Rev. A* **79**, 061601 (2009).
36. T.-L. Ho, Q. Zhou, *Proc. Natl. Acad. Sci. U.S.A.* **106**, 6916–6920 (2009).
37. A. M. Rey *et al.*, *Europhys. Lett.* **87**, 60001 (2009).
38. S. Trebst, U. Schollwöck, M. Troyer, P. Zoller, *Phys. Rev. Lett.* **96**, 250402 (2006).
39. S. Nascimbène *et al.*, *Phys. Rev. Lett.* **108**, 205301 (2012).
40. M. Lubasch, V. Murg, U. Schneider, J. I. Cirac, M.-C. Bañuls, *Phys. Rev. Lett.* **107**, 165301 (2011).
41. T. Senthil, A. Vishwanath, L. Balents, S. Sachdev, M. P. A. Fisher, *Science* **303**, 1490–1494 (2004).
42. M. F. Parsons *et al.*, *Science* **353**, 1253–1256 (2016).
43. L. W. Cheuk *et al.*, *Science* **353**, 1260–1264 (2016).

ACKNOWLEDGMENTS

We acknowledge help by K. Kleinlein and M. Lohse during the setup of the experiment and financial support by Max-Planck-Gesellschaft and the European Union [Ultracold Quantum Matter (UQUAM) and Quantum Simulation of Many-Body Physics in Ultracold Gases (QUSIMGAS)]. The data that support the plots within this paper and other findings of this study are available from the corresponding author upon reasonable request.

SUPPLEMENTARY MATERIALS

www.sciencemag.org/content/353/6305/1257/suppl/DC1
Supplementary Text
Figs. S1 to S5
Table S1
References (*44*–*51*)

17 May 2016; accepted 18 August 2016
10.1126/science.aag1635

QUANTUM SIMULATION

Observation of spatial charge and spin correlations in the 2D Fermi-Hubbard model

Lawrence W. Cheuk,[1]* Matthew A. Nichols,[1]* Katherine R. Lawrence,[1] Melih Okan,[1] Hao Zhang,[1] Ehsan Khatami,[2] Nandini Trivedi,[3] Thereza Paiva,[4] Marcos Rigol,[5] Martin W. Zwierlein[1]†

Strong electron correlations lie at the origin of high-temperature superconductivity. Its essence is believed to be captured by the Fermi-Hubbard model of repulsively interacting fermions on a lattice. Here we report on the site-resolved observation of charge and spin correlations in the two-dimensional (2D) Fermi-Hubbard model realized with ultracold atoms. Antiferromagnetic spin correlations are maximal at half-filling and weaken monotonically upon doping. At large doping, nearest-neighbor correlations between singly charged sites are negative, revealing the formation of a correlation hole, the suppressed probability of finding two fermions near each other. As the doping is reduced, the correlations become positive, signaling strong bunching of doublons and holes, in agreement with numerical calculations. The dynamics of the doublon-hole correlations should play an important role for transport in the Fermi-Hubbard model.

A central question in the study of cuprate high-temperature superconductors is how spin and charge correlations give rise to the wealth of observed phenomena. Antiferromagnetic order present in the absence of doping quickly gives way to superconductivity upon doping with holes or electrons (*1*), suggesting the viewpoint of competing phases. On the other hand, antiferromagnetic correlations can also occur in the form of singlet bonds between neighboring sites. In fact, it has been proposed (*2*) that superconductivity could result, upon doping a Mott insulator, from the condensation of such resonating valence bonds. It has also been argued (*1*) that the pseudogap and "strange metal" regions are supported by a liquid of spin-singlets. This argument has spurred the simultaneous examination of nearest-neighbor spin and charge correlations, which might reveal the underlying mechanisms of pairing and transport.

In recent years, ultracold atomic gases have been established as pristine quantum simulators of strongly correlated many-body systems (*3*–*5*). The Fermi-Hubbard model is of special importance, thanks to its paradigmatic role for the study of high–critical temperature cuprates. At low temperatures and away from half-filling, solving the Fermi-Hubbard model theoretically is very challenging because of the fermion sign problem. Central properties of Fermi-Hubbard physics—from the reduction of double occupancy (*6*, *7*) and of compressibility (*8*, *9*) as the repulsion is increased, to short-range antiferromagnetic correlations (*10*–*12*) and the equation of state (*9*, *13*, *14*)—have been observed in ultracold atom experiments. The recently developed Fermi gas microscopes (*13*, *15*–*19*) have led to the direct observation of two-dimensional (2D) fermionic Mott insulators, band insulators, and metals with single-atom, single-site–resolved detection (*20*, *21*). The strength of this technique, however, is on full display when single-site detection is used to directly measure correlations in the gas, as has been achieved with bosons (*22*–*24*).

[1]Department of Physics, MIT-Harvard Center for Ultracold Atoms, and Research Laboratory of Electronics, Massachusetts Institute of Technology (MIT), Cambridge, MA 02139, USA. [2]Department of Physics and Astronomy, San José State University, San José, CA 95192, USA. [3]Department of Physics, The Ohio State University, Columbus, OH 43210, USA. [4]Instituto de Fisica, Universidade Federal do Rio de Janeiro, Caixa Postal 68.528, 21941-972 Rio de Janeiro, RJ, Brazil. [5]Department of Physics, The Pennsylvania State University, University Park, PA 16802, USA.
*These authors contributed equally to this work. **†Corresponding author. Email: zwierlein@mit.edu**

Spin- and density-resolved microscopy of antiferromagnetic correlations in Fermi-Hubbard chains

Martin Boll, Timon A. Hilker, Guillaume Salomon, Ahmed Omran, Jacopo Nespolo, Lode Pollet, Immanuel Bloch and Christian Gross

Science **353** (6305), 1257-1260.
DOI: 10.1126/science.aag1635